

TECHNIQUE FOR DETERMINATION OF SURFACE FRACTAL DIMENSION AND MORPHOLOGY OF MESOPOROUS TITANIA USING DYNAMIC FLOW ADSORPTION AND ITS CHARACTERIZATION

Silvester Tursiloadi

The Research Centre for Chemistry - Indonesian Institute of Sciences, Kawasan Puspiptek Serpong, Tangerang, Indonesia
15314

Received September 17, 2008; Accepted March 3, 2009

ABSTRACT

A technique to determine the surface fractal dimension of mesoporous TiO_2 using a dynamic flow adsorption instrument is described. Fractal dimension is an additional technique to characterize surface morphology. Surface fractal dimension, a quantitative measurement of surface ruggedness, can be determined by adsorbing a homologous series of adsorbates onto an adsorbent sample of mesoporous TiO_2 . Titania wet gel prepared by hydrolysis of Ti-alkoxide was immersed in the flow of supercritical CO_2 at 60 °C and the solvent was extracted. Mesoporous TiO_2 consists of anatase nano-particles, about 5nm in diameter, have been obtained. After calcination at 600 °C, the average pore size of the extracted gel, about 20nm in diameter, and the pore volume, about $0.35\text{cm}^3\text{g}^{-1}$, and the specific surface area, about $58\text{m}^2\text{g}^{-1}$. Using the N_2 adsorption isotherm, the surface fractal dimension, D_s , has been estimated according to the Frenkel-Halsey-Hill (FHH) theory. The N_2 adsorption isotherm for the as-extracted aerogel indicates the mesoporous structure. Two linear regions are found for the FHH plot of the as-extracted aerogel. The estimated surface fractal dimensions are about 2.49 and 2.68. Both of the D_s values indicate rather complex surface morphology. The TEM observation shows that there are amorphous and crystalline particles. Two values of D_s may be attributed to these two kinds of particles. The two regions are in near length scales, and the smaller D_s , $D_s = 2.49$, for the smaller region. This result indicates that there are two kinds of particles, probably amorphous and anatase particles as shown by the TEM observation.

Keywords: surface fractal dimensions, CO_2 supercritically extraction, sol-gel, aerogel, titania

INTRODUCTION

Where classical geometry deals with objects of integer dimensions, fractal geometry describes non-integer dimensions. Zero dimensional points, one dimensional lines and curves, two dimensional plane figures like squares and circles, and three dimensional solids such as cubes and spheres make up the world as we have previously understood it. However, many natural phenomena are better described with a non-integer dimension between two whole numbers. While a straight line has a dimension of one, a fractal curve will have a dimension between one and two depending on how much space it takes up as it twists and curves [1]. The more that flat fractal fills a plane, the closer it approaches two dimensions. Likewise, a "hilly fractal scene" will reach a dimension somewhere between two and three. So a fractal landscape made up of a large hill covered with tiny bumps would be close to the second dimension, while a rough surface composed of many medium-sized hills would be close to the third dimension [1].

A mathematical strategy for describing rugged or indeterminate boundaries was developed by Mandelbrot and is known as fractal geometry [2-4]. The surface fractal dimension, D , is an intrinsic quantitative measure of

surface irregularity; it is bounded between the topological dimension of 2 and the Euclidian dimension of 3. Several techniques have been suggested to determine the fractal dimension [5,17-21] with experimental techniques including image analysis and gas adsorption, predominating. Using the N_2 adsorption isotherm, the surface fractal dimension, D_s , has been estimated according to the Frenkel-Halsey-Hill (FHH) theory. Equations (1) and (2) have been used.

$$\ln(V/V_0) = (-1/m) \ln[(P_0/P)] + \text{constant} \quad (1)$$

$$D_s = 3 - (1/m) \quad (2)$$

where V , V_0 and P/P_0 are the adsorbed volume of N_2 , the saturation volume of adsorbed N_2 and the relative pressure, respectively [6].

The adsorption data are measured using a micromeritics, Tristar 3000, continuous flow surface area analyzer. The samples for analyzed were prepared by sol-gel method. One of the most important applications of the sol-gel method can be found in the field of catalysts. The most common sol-gel process involves the controlled hydrolysis of metal alkoxide precursor followed by condensation to form a three-dimensional gel network. The high porosity and the high specific surface area of material prepared by the sol-gel method make them very attractive from catalytic point of view. Titania is known to have polymorphs;

* Corresponding author.
Email address : tursilo@gmail.com

anatase, rutile, and brookite. Anatase has been extensively investigated owing to its notable functions for photo catalysis and photon-electron transfer [7, 8]. However, the disadvantage of titania for photo catalysis material is relatively low surface area, the low porosity and high temperature anatase formation. The most common pure anatase phase have small specific surface area that is less than $55 \text{ m}^2/\text{g}$ [6], and anatase formation at temperature higher than $400 \text{ }^\circ\text{C}$ [9, 10]. The supercritical extraction technique seems to be a good alternative to overcome the problems of high temperature anatase formation, low porosity and low surface area of anatase. Supercritical extraction techniques are recently used in material science to fabricate highly porous materials [11].

In this study, surface fractal dimension and surface morphology of mesoporous TiO_2 using a dynamic flow adsorption instrument and TEM were analyzed. Titania wet gel prepared by hydrolysis of Ti-alkoxide was immersed in the flow of supercritical CO_2 at $60 \text{ }^\circ\text{C}$ and the solvent was extracted. The surface morphology of titania nanoparticles has been discussed with the surface fractal dimensions from the N_2 adsorption isotherm.

EXPERIMENTAL SECTION

Wet gels of TiO_2 were prepared by hydrolysis of titanium n-butoxide, $\text{Ti}(\text{O}-n\text{-C}_4\text{H}_9)_4$ (TNB) in a methanol solution with acid catalyst. The molar ratios used for the synthesis was TNB: H_2O : methanol: HNO_3 = 1:13.4:127:0.06. Firstly, TNB was dissolved into a mixture of methanol and small amount of H_2O at room temperature. After stirring for 30 min, the catalyst solution of methanol, H_2O and HNO_3 was added to the TNB solution under continuous stirring. The solution gelled in 2 min. The gel time was defined as the time required after mixing for the vortex created by the stirring to disappear completely. The wet gel was aged at room temperature for 18h and extracted by flowing supercritical carbon dioxide, flowing CO_2 of 5.5 Lt min^{-1} in a supercritical extraction system at $60 \text{ }^\circ\text{C}$ and 22Mpa for 4h.

Crystallization behaviors of the gels were investigated with X-ray diffractometer (Rigaku, RAD-C) and electron diffractometry by a transmittance electron microscopy (TEM, Philips, Tecnai F20) after calcination at 500, 600, 700, and $800 \text{ }^\circ\text{C}$ with heating rate of $10 \text{ }^\circ\text{C.min}^{-1}$, holding time of 2 h and a cooling rate of $10 \text{ }^\circ\text{C.min}^{-1}$. The grain sizes of the samples were estimated from the images observed by TEM. The specific surface area, pore size distribution, and pore volume of gels, before and after calcinations, were estimated by the Barret-Joyner-Halenda (BJH) method using N_2 adsorption-desorption curves (Micromeritics, Tristar 3000) [12].

The techniques to determine the fractal dimension of surfaces using N_2 gas adsorption isotherm, the surface fractal dimension, D_s , has been estimated according to the Frenkel-Halsey-Hill (FHH) theory [13, 14]. Equations (1) and (2) have been used.

$$\ln(V/V_0) = (-1/m) \ln[\ln(P_0/P)] + \text{constant} \quad (1)$$

$$D_s = 3 - (1/m) \quad (2)$$

where V , V_0 and P/P_0 are the adsorbed volume of N_2 , the saturation volume of adsorbed N_2 and the relative pressure, respectively. This technique uses gas adsorption data to determine the pore volume distribution. The change in cumulative pore volume with respect to pores of radius is related to the fractal dimension.

RESULT AND DISCUSSION

X-ray powder diffraction of anatase was found for as-extracted aerogel (Fig. 1). The anatase structure was stable after calcination up to $500 \text{ }^\circ\text{C}$. After calcination at $600 \text{ }^\circ\text{C}$, small diffraction peaks of rutile were found. After calcination $600 \text{ }^\circ\text{C}$, the anatase peaks almost disappeared and strong peaks of rutile were found.

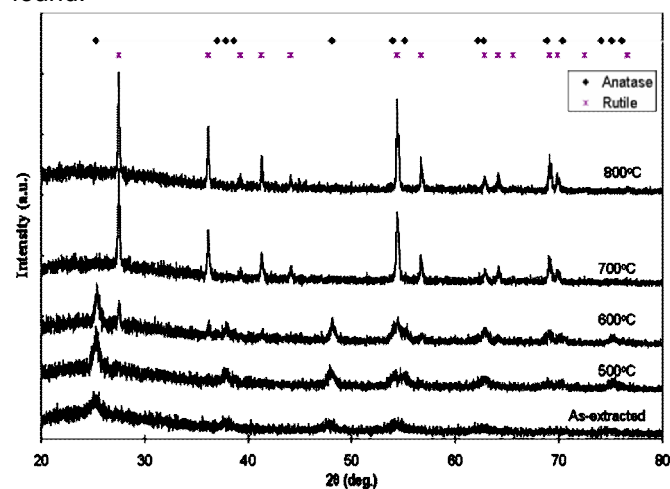


Fig 1. XRD patterns of the titania aerogel at various temperatures

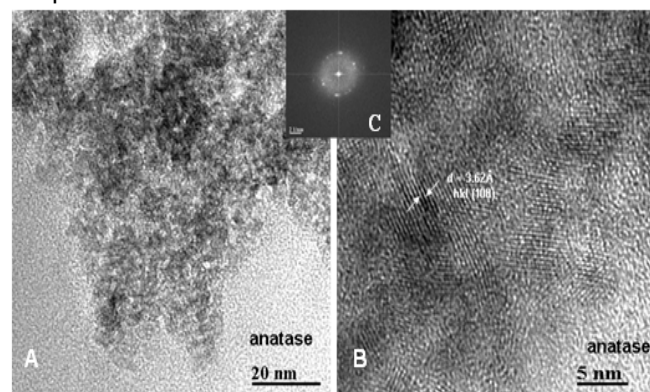


Fig 2. TEM images, (A) and (B), and electron diffraction pattern (C) of the as-extracted titania aerogel

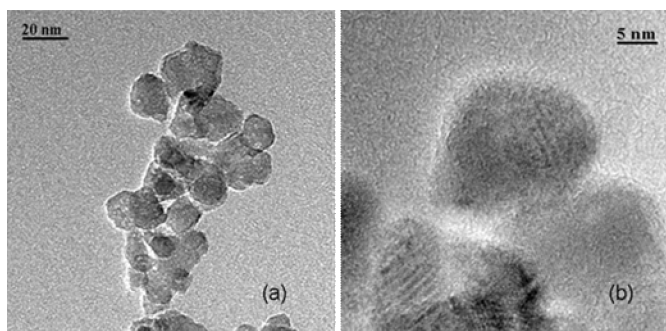


Fig 3. TEM images of the aerogel calcined at 500 °C

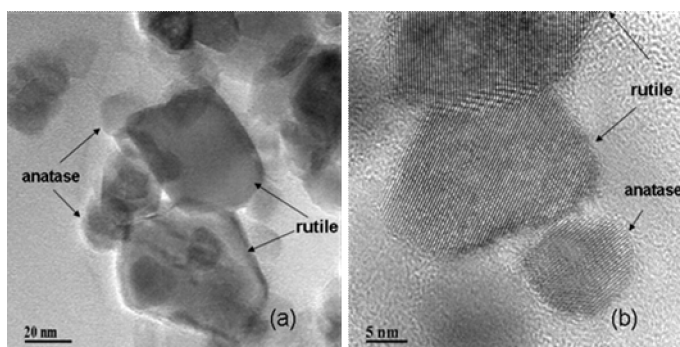


Fig 4. TEM images of the aerogel calcined at 600 °C

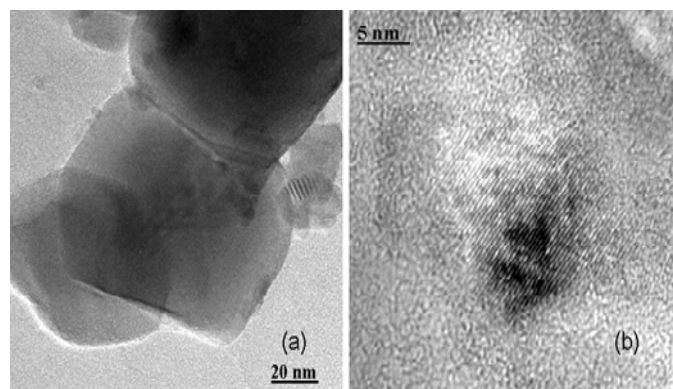


Fig 5. TEM images of the aerogel calcined at 700 °C

Table 1. Nanocrystalline anatase particles (nm) after calcination at various temperatures

Temperature (°C)	Titania aerogel (in diameter)
As-extracted	5
500	13
600	13
700	(25 = rutile) 90*

Table 2. Specific surface area, cumulative pore volume, and average pore diameter of the titania gels after calcination at various temperatures.^a

	60 °C	500 °C	600 °C	700 °C	800 °C
Surface area ($\text{m}^2 \text{g}^{-1}$)	195	90	58	19	5
Pore volume ($\text{cm}^3 \text{g}^{-1}$)	0.55	0.49	0.35	0.16	0.05
Average pore diameter (nm)	12.8	18.7	20.0	36.5	51.6

^a The accuracy of N_2 adsorption measurements was 0.1 %, and the reproducibility of these values for each sample was within 10 %.

Figures 2 – 5 show the TEM images and electron diffraction patterns of the aerogels. Small grains, 5nm in diameter, with anatase structure were observed for the as-extracted gel along with amorphous nano-particles (Fig. 2, Table 1). The grain size of the aerogel increases significantly about to 13 nm, after calcination at 500 °C (Fig. 3 and Table 1). After calcination at 600 °C, two kinds of particles, anatase about 13 nm in diameter and rutile about 25 nm, were observed (Fig. 4, Table 1). After calcination at 700 °C, only rutile particles were found, and the size increased drastically up to 90nm (Fig. 5, Table 1).

Table 2 shows the effect of calcination temperatures on specific surface area, cumulative pore volume, and average pore diameter of TiO_2 gels. After calcination at 500 °C, the specific surface area of the aerogel, about $90 \text{m}^2 \text{g}^{-1}$. After calcination at 600 °C, the specific surface area of the aerogel was still large, about $58 \text{m}^2 \text{g}^{-1}$. The cumulative pore volume of the aerogel

gradually decreased with increasing calcinations temperatures up to 700 °C. The average pore size of the aerogel increased with increasing calcinations temperature. Fig. 6 shows the pore size distribution of TiO_2 gels.

Figures 7 and 8 show the examples of the FHH plot of the N_2 adsorption- desorption isotherms. From the linear region of the FHH plot, surface fractal dimensions of the calcined gels have been estimated and show in table 2. Two linear regions were found only for the as-extracted aerogel. The surface fractal dimensions of the aerogels calcined at 700 °C or higher temperatures and of the xerogel calcined at 500 °C or higher temperatures cannot be estimated by this method because of the small surface area.

Using the one-step supercritical extraction technique, a material with a large specific surface area and high porosity can be obtained. In addition, amorphous titania crystallizes at low temperature in su-

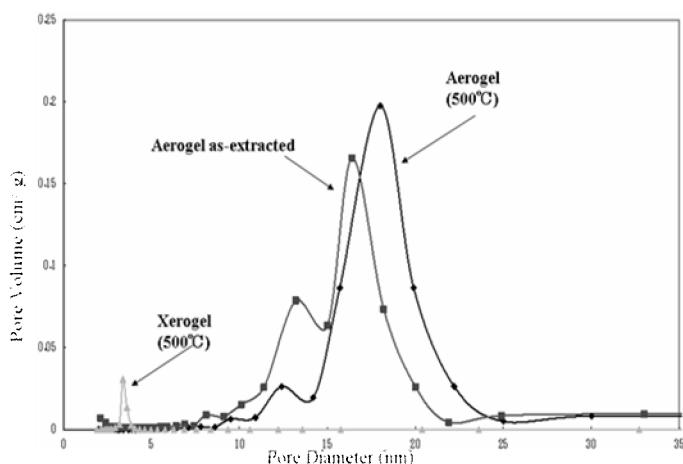


Fig. 6. Pore size distribution of gels as-extracted and after calcination at 500 °C

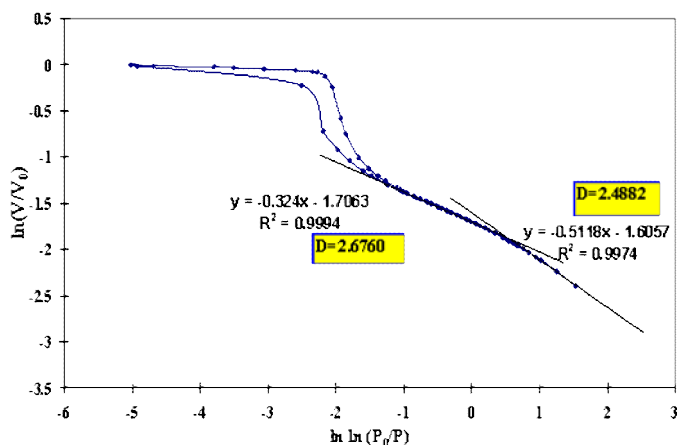


Fig 7. Frenkel-Halsey-Hill plot of the as-extracted aerogel

percritical CO₂ fluid resulting in anatase nano-particles, about 5nm in diameter. The conventional unit cell of titania in the anatase structure is shown in Fig. 9. Anatase nano-particles were found in the as-extracted aerogel along with amorphous particles (Fig. 2 and 1). Under a high pressure (22 MPa), anatase nano-particles were formed at low temperature (60 °C). During supercritical extraction, anatase deposited, probably through the solution-deposition mechanism, in the supercritical fluid of CO₂. At low temperature, the growth rate of anatase crystals was low, and the gel consisted of nano-particles was obtained.

The specific surface area, average pore diameter and pore volume of the as-extracted aerogel were 195 m²g⁻¹, 12.8 nm and 0.55 cm³g⁻¹, respectively, and they changed to 90 m²g⁻¹, 18.7 nm and 0.49 cm³g⁻¹ after calcination at 500 °C (Table 2). Diameter of anatase after calcination at 500 °C (table.1) was smaller than average pore diameter (table 2). This result shows that agglomeration was occurred (Fig. 13). The change of

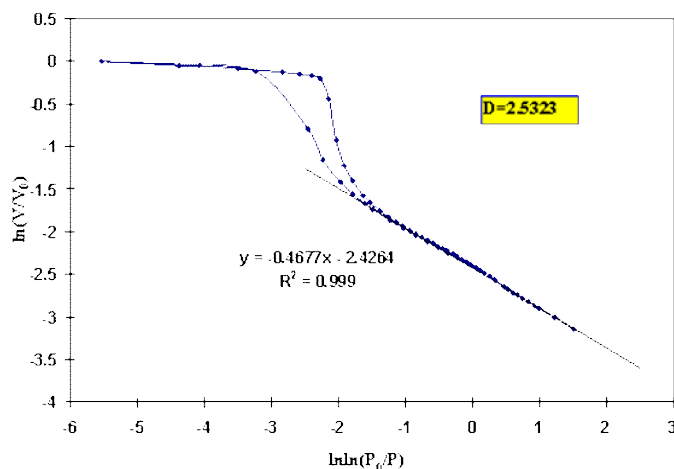


Fig 8. Frenkel-Halsey-Hill plot of the aerogel calcined 600 °C

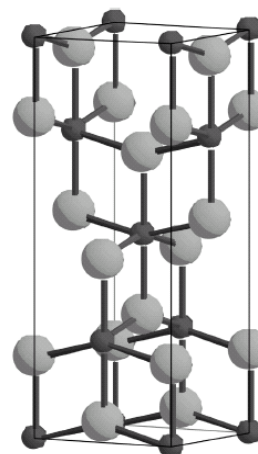


Fig. 9 Ball and sticks view of the TiO₂ conventional unit cell in the anatase structure. Dark gray and white balls correspond to titanium and oxygen atoms, respectively.

pore volume by calcination at 500 °C was not significant, from 0.55 cm³g⁻¹ to 0.49 cm³g⁻¹. This result shows that the porous structure of the aerogel was stable at 500 °C. The drastic decrease in specific surface area may be due to the crystal growth of anatase, from ca. 5nm to ca. 13nm in diameter (Figs. 2 and 3). The surface fractal dimension of the aerogel calcined at 500 °C, $D_s = 2.55$, was slightly larger than that of the xerogel, $D_s = 2.49$ (Table 3). This result shows that the surface structure of the aerogel and of the xerogel is slightly different. The aerogel has more complex surface, and may have a larger specific surface area.

After calcination at 600 °C, the pore volume of the aerogel drastically decreased to 0.35 cm³g⁻¹ (Table 2). After calcination at 600 °C, the average pore diameter to 20 nm and the specific surface area of the aerogel decreased to 58 m²g⁻¹. These results may be attributed to sintering along with the phase transformation from anatase to rutile. The specific surface area dropped to

$19 \text{ m}^2 \text{ g}^{-1}$ and the pore diameter increased drastically to 36.5nm after calcination at 700 °C due to rutile crystal growth, and the particle size increased up to 90 nm. The pore volume drastically decreased to $0.16 \text{ cm}^3 \text{ g}^{-1}$. These results show that sintering and grain growths proceed with phase transformation from anatase to rutile. The spherical anatase particles are small, around 13nm in diameter after calcination at 500 °C (Fig. 3), and the hexagonal rutile particles are large, around 90nm in diameter after calcination at 700 °C (Fig. 5). Thus, the surface area of the aerogel remarkably decreases with the phase transformation from anatase to rutile.

The phase transformation temperature from anatase to rutile for the aerogel is slightly higher than that for the xerogels in general and particle size of anatase aerogel is smaller than that of the xerogel in same calcination temperature. It is indicated that small particle has low surface energy and more stable. After calcination at 600 °C, diffraction peaks of anatase were strong for the aerogel (Fig. 1). As discussed previously, the surface of the aerogel is more complex and particle size is smaller. The difference in the surface morphology and particle size may affect the stability of anatase nanoparticles and the phase transformation temperature. The above calcination experiments of titania aerogel indicate that higher temperature, anatase transform to rutile. Author considers this to be a consequence of the dependence of thermodynamic stability on particle size, noting that aerogel and xerogel in general growth rates differ, causing changes in relative stability during thermal treatments. Table 1 illustrates the nanocrystalline anatase particles (nm) after calcination at various temperatures. It is seen that, at particle size equal or less than 13 nm, anatase is the most stable phase; for particles sizes greater than 13 nm, rutile is the most stable phase. The particle coarsening rate was proportional to the rate of transformation and higher temperature runs contain more rutile (Table 1). Thus, it is clear that the high temperature results are overstate the anatase size when rutile first formed. Given this consideration, anatase size data in Table 1 consistently indicate the critical size at which anatase starts to transform to rutile is around 13 nm. The critical size of anatase may arise from kinetic effects or thermodynamic constraint. If it is due to kinetic effects, i.e., the activation energy of the transformation is related to the particle size in some way, it is expected that this size varies greatly with temperature, because a change in temperature can significantly change the kinetic energy of atoms in nanocrystalline anatase. The Gibb's free energy is difference between the amorphous and crystalline phases or between two crystalline phases [15, 16]. Surface free energy constitutes a large part of the total free energy of substances of ultrafine particle sizes. The theoretical prediction depends upon the fact that rutile has higher surface energy than anatase.

Table 3. Surface fractal dimension, D_s , of titania gels

Sample	Calcination Temperature	D_s
Aerogel	As-extracted (60 °C)	2.68, 2.49
	500 °C	2.55
	600 °C	2.53
Xerogel	500 °C	2.49

The surface morphology of the gels was evaluated with the surface fractal dimension, D_s , estimated from the N_2 adsorption isotherms. The N_2 adsorption data are plotted according to Eq. (1) in Figs. 7 and 8, FHH plot and the D_s value are estimated with Eq. (2). The N_2 adsorption isotherm for the as-extracted aerogel indicates the mesoporous structure. Two linear regions are found for the FHH plot of the as-extracted aerogel (Fig. 7). The estimated surface fractal dimensions are about 2.49 and 2.68. Both of the D_s values indicate rather complex surface morphology. The TEM observation shows that there are amorphous and crystalline particles. Two values of D_s may be attributed to these two kinds of particles. The two regions are in near length scales, and the smaller D_s , $D_s = 2.49$, for the smaller region (Fig. 7). This result indicates that there are two kinds of particles, probably amorphous and anatase particles as shown by the TEM observation (Fig. 2). The value of smaller D_s was near to that of the sample calcined at 500 °C, $D_s = 2.55$ for the aerogel and $D_s = 2.49$ for the xerogel (Table 3), and that of polycrystalline porous anatase, about 2.44, reported by B. Yao, et al. [14]. It may be expected that crystalline particles have smoother surface with smaller surface fractal dimension. Thus the smaller particles may be crystalline, anatase. The low growth rate at low temperature, 60 °C, results in the formation of small crystalline particles. These results, difference in the surface fractal dimensions, show the differences in the surface roughness between the amorphous titania nanoparticles and the anatase nanoparticles. In the length scale up to ca. 13nm, D_s was about 2.5 for the crystalline samples calcined at 500 °C or higher temperatures (Fig. 8). These values indicate that the crystalline mesoporous titania has rather complex shape of surface. After calcining at 600 °C, the crystalline particles growth larger, but the change in D_s is not significant (Fig. 8). This result shows the surface roughness of anatase particles hardly changed by calcination.

CONCLUSION

The fractal analysis using N_2 adsorption isotherm makes it possible to evaluate surface morphology in nanometer scale. Fractal dimensions for the mesoporous titania prepared by CO_2 supercritical extraction technique will provide a new route for obtaining mesoporous anatase with nano-scale grain size. These

results, difference in the surface fractal dimensions, show the differences in the surface roughness between the amorphous titania nanoparticles and the anatase nanoparticles. In the length scale up to ca. 13nm, D_s was about 2.5 for the crystalline samples calcined at 500 °C or higher temperatures. These values indicate that the crystalline mesoporous titania has rather complex shape of surface. After calcining at 600 °C, the crystalline particles growth larger, but the change in D_s is not significant. This result shows the surface roughness of anatase particles hardly changed by calcination.

The porous structure of anatase was fairly stable at temperature up to 500 °C. Supercritical extraction using CO₂ induced low temperature crystallization of titania gels. Nanoparticles of anatase, less than 13 nm in diameter, can be obtained at low temperatures. It is seen that, at particle size equal or less than 13 nm, anatase is the most stable phase; for particles sizes greater than 13 nm, rutile is the most stable phase.

REFERENCES

1. Oki, Yasuyuki, Koike, Hironobu and Takeuchi, Yoshiaki, *US patent*, Serial No.: 978004, Application Number , 11-228474J. 2002.
2. Mandelbrot, B.B., *The Fractal Geometry of Nature*, W.H. Freeman and Company, New York, 1983
3. Barnsly, M., *Fractals Everywhere*, Academic Press, Inc., New York, 1988.
4. Vicsek, T., *Fractal Growth Phenomena*, World Scientific, London, 1989.
5. Avnir, D., *Proceeding Materials Research Society Symposium*, Vol. 73, *Better Ceramics Through Chemistry II*, Materials Research Society, Pittsburgh, PA, 1986, p. 321.
6. Haerudin, H., Bertel, S., and Kramer, R., 1998, *J. Chemical Society, Faraday Trans*, **94** (10), 1481.
7. Fox, M.A. and Dulay, M.T., *Chem. Rev.*, **93**, 1993, 341.
8. Moritz, T., Reiss, J., Diesner, K., Su D., and Chemseddine, A., *J. Phys. Chem. B*, **101**, 1997, 8052.
9. Hirashima, H., Imai, H., and Balek, V., *J. Non-Crystalline Solids*, **285**, 2001, 96.
10. Yusuf, M.M., Imai, H., Hirashima, H., 2001, *J. Non-Crystalline Solids*, **285**, 90.
11. Suh, D.J., Park, T.J., Kim, J.H., and Kim, K.L., *Chem. Mater.* **9**, 1997, 1903.
12. Barret, E.P., Joyner, L.G. and Halenda, P.H., 1951, *J. Am. Chem. Soc.*, **73**, 373.
13. Imai, H., Morimoto, H., Tomonaga, A., and Hirashima, H., 1997, *J. Sol-gel Sci. and Tech.*, **10**, 45
14. Yao, B., Zhang, Y., Shi, H., and Zhang, L., 2000, *Chem. Mat.*, **12**, 3740.
15. Kasuga, T., Hiramatsu, M., Hoson, A., Sekino, T., and Niihara, K., 1999, *Adv. Mater.*, **11**, 1307.
16. Kumar, K-N.P., Keizer, K., Burggraaf, A.J., Okubo, T., and Nagamoto, H., 1993, *J. Mater. Chem.*, **3**, 1151.
17. Fan, K. and Hatzkiriokos, S.G., *Wood Science and Technology*, **33**, 1999, 139-145.
18. Staszczuk, P., Sternik, D., and Chadzynski, G.W., 2003, *Journal of Thermal analysis and Calorimetry*, **71**, 173-182.
19. Balovsyak, S.V., Fodchuk, I.M., and Lytvyn, P.M., 2003, *Semiconductor Physics, Quantum Electronics & Optoelectronics*, **6**, 41-46
20. Staszczuk, P., Matyjewicz, M., Kowalska, E., Radomska, J., Byszewski, P., and Kozlowwski, M., 2003, *Rev. Adv. Mater. Sci.* **5**, 471-476.
21. HongWei, F., MingHong, C., and ZhiHe, C., 2008, *Sci. China. Ser. G-Phys. Astron.*, **51**, 8, 1022-1028